THE JOURNAL OF PHYSICAL CHEMISTRY B

Article

pubs.acs.org/JPCB

Open Access on 08/14/2015

Sodium Dodecyl Sulfate Monomers Induce XAO Peptide Polyproline II to α-Helix Transition

Zhenmin Hong, Krishnan Damodaran, and Sanford A. Asher*

Department of Chemistry, University of Pittsburgh, Pittsburgh, Pennsylvania 15260, United States

Supporting Information

ABSTRACT: XAO peptide ($Ac-X_2A_7O_2-NH_2$; X: diaminobutyric acid side chain, $-CH_2CH_2NH_3^+$; O: ornithine side chain, $-CH_2CH_2CH_2NH_3^+$) in aqueous solution shows a predominantly polyproline II (PPII) conformation without any detectable α-helix-like conformations. Here we demonstrate by using circular dichroism (CD), ultraviolet resonance Raman (UVRR) and nuclear magnetic resonance (NMR) spectroscopy that sodium dodecyl sulfate (SDS) monomers bind to XAO and induce formation of α-helix-like conformations. The stoichiometry and the association constants of SDS and XAO were determined from the XAO−SDS diffusion coefficients measured by pulsed field gradient NMR. We developed a model for the formation of XAO−SDS aggregate α-helix-like conformations. Using UVRR spectroscopy, we calculated the Ramachandran ψ angle distributions of aggregated XAO peptides. We resolved α-, π- and 3_{10}- helical conformations and a turn conformation. XAO nucleates SDS aggregation at SDS concentrations below the SDS critical micelle concentration. The XAO_4-SDS_{16} aggregates have four SDS molecules bound to each XAO to neutralize the four side chain cationic charges. We propose that the SDS alkyl chains partition into a hydrophobic core to minimize the hydrophobic area exposed to water. Neutralization of the flanking XAO charges enables α-helix formation. Four $XAO-SDS_4$ aggregates form a complex with an SDS alkyl chain-dominated hydrophobic core and a more hydrophilic shell where one face of the α-helix peptide contacts the water environment.

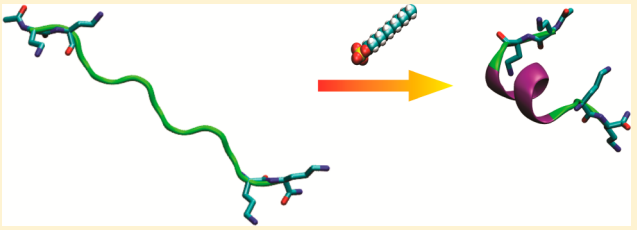

INTRODUCTION

The aggregation and fibrillation of some intrinsically disordered proteins (IDPs)[1] appear to be involved in the development of neurodegenerative disorders such as Parkinson's disease, Alzheimer's disease, and type II diabetes.[2−4] It has been proposed that α-helix-like conformations are important intermediates during amyloid fibril formation.[5−7] Some IDPs form α-helix-like conformations upon association with membranes through a mechanism that involves further aggregation and fibrillation. For example, α-synuclein (αS, associated with Parkinson's disease) upon binding to membranes or surfactant micelles forms α-helices that appears to mediate αS aggregation and fibrillation.[8−11] For amyloid β-peptide (Aβ, associated with Alzheimer's disease), the monomer peptide binds to surfactant micelles[12,13] and lipid membranes,[14,15] forming α-helix-like conformations that facilitate aggregation and fibrillation.[16] Similar phenomena occur for other IDPs, such as medin[17] and islet amyloid polypeptide (IAPP, associated with type II diabetes).[18,19]

IDPs protofibrils or oligomeric aggregates are more toxic than are the insoluble fibrils.[2,20] Recently, it was shown that the toxic IDPs protofibrils or oligomeric aggregates form pores in membranes, apparently sharing a common mechanism with antimicrobial peptides (AMPs).[21−23] When AMPs are associated with anionic lipid membranes, many of them also form α-helix-like conformations[24−28] that display antimicrobial activity.[29−31]An understanding of the α-helix formation mechanism of these peptides would help understanding the overall fibrillation mechanism of these IDPs, as well as help in the design of AMPs.

In this paper, we study the interactions between an undecapeptide XAO ($Ac-X_2A_7O_2-NH_2$; MW = 985; X: diaminobutyric acid (Dab) side chain, $-CH_2CH_2NH_3^+$; O: ornithine (Orn) side chain, $-CH_2CH_2CH_2NH_3^+$) with sodium dodecyl sulfate (SDS). The XAO peptide was chosen because (1) it has a large content of hydrophobic residues (seven Ala) and multiple cationic residues (two Dab and two Orn), similar to many of those IDPs and AMPs. Uversky[32,33] proposed a simple relationship between mean hydrophobicity and mean net charge to predict whether a peptide sequence is intrinsically disordered or natively folded. The XAO has a mean hydrophobicity of 0.47 and a mean net charge of 0.36, indicating that XAO should be intrinsically disordered. (2) In aqueous solution, monomeric XAO predominantly adopts a polyproline II (PPII) conformation,[34,35] similar to that of some IDPs[36−38] and AMPs.[39] XAO does not exhibit any detectable α-helical content, presumably due to its short polyAla repeat length and electrostatic repulsion between its flanking cationic Dab and Orn side chains. The structural similarities between XAO and some IDPs/AMPs make XAO a relevant model to

Received: April 28, 2014
Revised: July 19, 2014
Published: August 14, 2014

   dx.doi.org/10.1021/jp504133m | J. Phys. Chem. B 2014, 118, 10565−10575

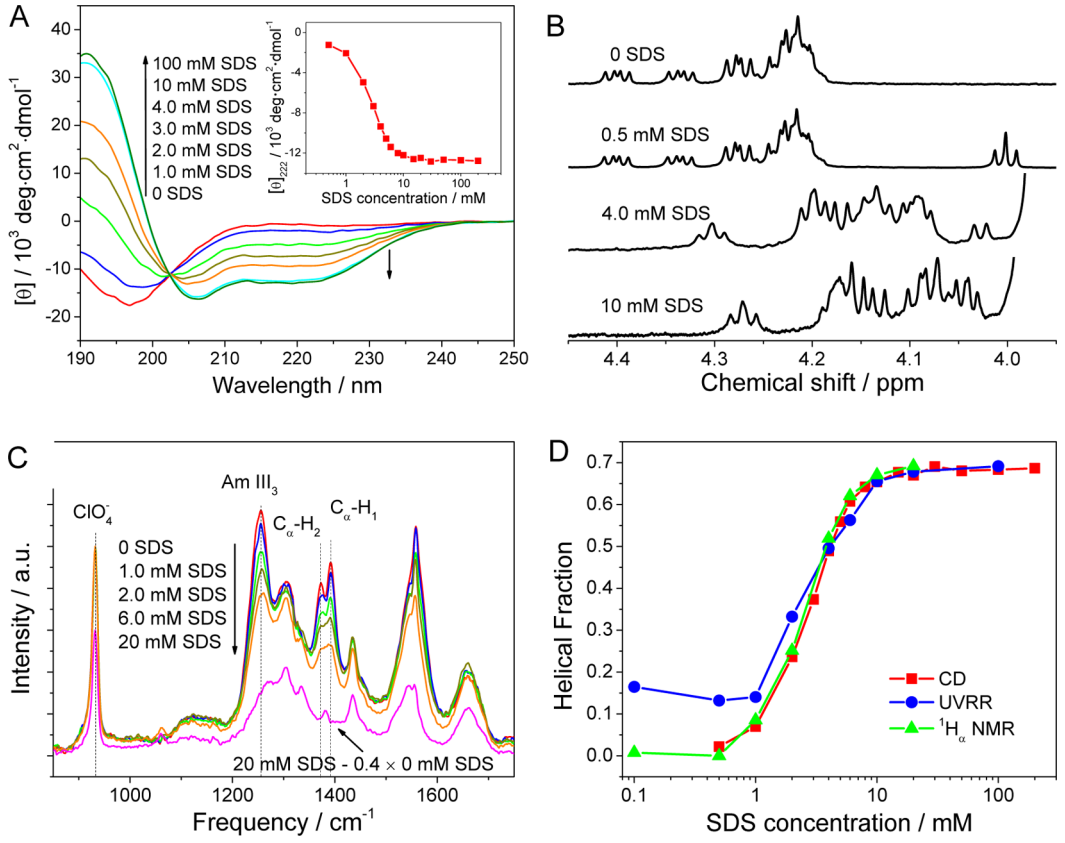

Figure 1. (A) CD spectra of 1.0 mM XAO in 0.1 M aqueous $NaClO_4$ solution at different SDS concentrations. The inset shows the dependence on the SDS concentration of the CD spectra 222 nm ellipticity. (B) $^1H_\alpha$ NMR spectra of XAO in 0.1 M $NaClO_4$ at different SDS concentrations. (C) 204 nm excited UVRR spectra of XAO in 0.1 M $NaClO_4$ at different SDS concentrations. The difference spectrum calculated emphasizes the Ala methyl group umbrella bending band at 1382 cm^{-1}. (D) SDS concentration dependence of the α-helical fraction of 1.0 mM XAO in 0.1 M $NaClO_4$ calculated from the CD, $^1H_\alpha$ NMR and UVRR spectra.

study mechanisms of interactions between these IDPs/AMPs and lipid membranes. SDS was chosen due to its amphiphilic molecular structure. SDS micelles have been widely used as a model membrane to study interactions between IDPs/AMPs and lipid membranes.[9,12,13,40−47]

We showed here that XAO adopts α-helix-like conformations upon aggregating with SDS. We used ultraviolet resonance Raman (UVRR) spectroscopy to determine the structure of the aggregated XAO.[48,49] We measured the diffusion coefficients of XAO and SDS by employing pulsed field gradient nuclear magnetic resonance (PFG-NMR). Based on the stoichiometry and association constants extracted from the diffusion coefficients, we propose a two-state model for the aggregation between XAO and SDS. This study demonstrates that SDS monomers bind to XAO, forming XAO−SDS aggregates that induce XAO α-helix-like conformations.

EXPERIMENTAL METHODS

Materials. The undecapeptide XAO was prepared by the Pittsburgh Peptide Facility by using a solid-state peptide synthesis method. SDS (99%), dodecyltrimethylammonium chloride (DTAC, 99%) and sodium perchlorate ($NaClO_4$, 98%) were purchased from Sigma-Aldrich Co. Sodium decylsulfate (SDeS, 99%), sodium octylsulfate (SOS, 99%) and sodium pentylsulfate (SPS, 99%) were purchased from Alfa Aesar. Sodium ethylsulfate (SES, 98%) was purchased from Tokyo Chemical Industry Co., Ltd. (TCI). Dodecylphosphocholine (DPC, 99%) and dodecyl-β-D-maltoside (DDM, 99%) were purchased from Avanti polar lipids, Inc. All chemicals were used as received unless specified otherwise. Water (18.2 MΩ·cm) was purified by a NANOPURE Infinity ultrapure water purifier. All samples contained 0.1 M $NaClO_4$ unless otherwise noted. Unless stated differently, the XAO concentration is 1.0 mM.

Circular Dichroism (CD) Measurements. CD spectra were measured by using a Jasco J-710 spectrometer. We used a temperature-controlled quartz cuvette with a 0.2 mm path length for 1.0 mg/mL (1.0 mM) samples. The temperature was controlled at 20 °C by an external water bath. The CD spectra were collected at 0.2 nm intervals and averaged over 5 scans and smoothed by the second order Savitzky-Golay method over 15 data points.

204 nm Excited UVRR Spectra. The UVRR instrumentation was described in detail previously.[50] Briefly, the third harmonic of a Nd:YAG laser (Coherent Infinity) was anti-Stokes Raman shifted five harmonics in 40 psi hydrogen gas to 204 nm. The 204 nm light is in resonance with the peptide bond first allowed $\pi-\pi^*$ electronic transition. The excitation beam was directed to a spinning quartz NMR tube containing the room temperature (~20 °C) sample solutions. The backscattered Raman light was collected and dispersed by a partially subtractive double monochromator and detected by a Lumogen coated back-thinned CCD detector (Princeton Instruments Spec-10:400B) that is cooled by liquid nitrogen. The sample UVRR spectra were obtained by subtracting appropriate amounts of water and the empty quartz NMR tube

dx.doi.org/10.1021/jp504133m | J. Phys. Chem. B 2014, 118, 10565−10575

UVRR from the raw spectra and normalized to the intensity of the 0.1 M $NaClO_4$ internal standard.

NMR Diffusion Measurements. All diffusion coefficient measurements were performed using a Bruker Avance III 600 MHz spectrometer with a BBFO Plus probe. The temperatures were controlled to ±1 °C accuracy using a Bruker BVT3000 temperature control system. The spectrometer was calibrated against the water self-diffusion coefficient at 25 °C. The samples were prepared in D_2O and the residual HOD resonance at δ = 4.70 was used as an internal chemical shift standard. Diffusion coefficients were determined using a stimulated echo pulsed field gradient pulse sequence with bipolar gradients.[51,52] To obtain the diffusion coefficient, the peak intensity versus gradient strength data were fit to the Stejskal−Tanner equation[53,54]

$$I = I_0 e^{-4\pi^2 D_s \gamma^2 G^2 \xi^2 (\Xi - \frac{\xi}{3})} \quad (1)$$

where I and I_0 are the intensities of a specific band (or the intensity at a specific chemical shift) with and without the magnetic field gradient; γ is the gyromagnetic ratio and equals 42.58 MHz·T^{-1} for ^{1}H nuclei; ξ and Ξ are the pulse width and pulse interval, D_s is the diffusion coefficient of the species in D_2O; and G is the gradient strength applied to the sample. Sixteen spectra were taken with gradient strengths that varied between 0 and 50 G/cm, while the duration of the gradient ξ was held constant throughout the experiment.

To plot the results as two-dimensional diffusion-ordered spectroscopy (DOSY) contours with respect to the chemical shift and diffusion coefficient, these 16 spectra were fitted to eq 1 to obtain $D_s(\delta)$ and the intensity $I_0(\delta)$ at each chemical shift δ. A normal distribution of intensities was generated along the diffusion coefficient axis at each chemical shift. The peak height, center position, and standard deviation of the normal distribution are labeled as $I_0(\delta)$, $D_s(\delta)$, and $\Delta D_s(\delta)$ (standard error of $D_s(\delta)$), respectively[55]

$$I(\delta, D) = I_0(\delta) e^{-(D - D_s(\delta))^2 / 2\Delta D_s(\delta)^2} \quad (2)$$

The integrated intensities of resonances from the same species were globally fit to obtain a single diffusion coefficient for qualitative analysis by using eq 1.

RESULTS AND DISCUSSION

CD Spectra of XAO in Different SDS Concentration Solutions. Figure 1A shows the CD spectra of XAO as a function of SDS concentration in 0.1 M $NaClO_4$ aqueous solutions at 20 °C. In the absence of SDS, the CD spectrum of XAO is similar to previously reported CD spectra of XAO in pure water or in low salt concentration solutions.[35,56,57] The CD spectra show characteristic PPII features such as the intense negative band at ∼197 nm. These features indicate that XAO adopts mainly a PPII-like conformation in 0.1 M $NaClO_4$ aqueous solutions in the absence of SDS. As the SDS concentration increases, the CD spectrum begins to show α-helix features, with two negative bands at 222 and 206 nm and a strong positive band at ∼190 nm. A well-defined isodichroic point occurs at 202 nm, indicating that XAO apparently undergoes a two-state transition from a PPII-like conformation to an α-helix-like conformation.

The negative mean residue ellipticity at 222 nm is proportional to the fraction of α-helix-like conformations

$$[\theta] = f_H([\theta]_H - [\theta]_P) + [\theta]_P \quad (3)$$

To calculate the α-helical fraction f_H, the 222 nm mean residue ellipticities of the α-helical state $[\theta]_H$ and the PPII state $[\theta]_P$ need to be determined. $[\theta]_P$ is the mean residue ellipticity of the XAO PPII-like conformation. This value can be obtained from the CD measurement of XAO in the absence of SDS.

The determination of $[\theta]_H$ is challenging, because it is difficult to force XAO to adopt a pure α-helix state. The commonly used strong α-helix promoting solvent trifluoroethanol (TFE) does not induce substantial amounts of α-helix. In a previous study,[57] the 222 nm mean residue ellipticity of XAO in TFE was measured to be −7000 deg·cm^2·dmol^{-1}, which is less negative than XAO in 10 mM SDS. The CD spectrum of XAO in TFE does not resemble the pure α-helix CD spectra, indicating that XAO does not exist in its pure α-helix conformation in TFE.

Another common approach[58,59] to estimate $[\theta]_H$ uses eq 4,

$$[\theta]_H = [\theta]_\infty (n - k)/n \quad (4)$$

where, $[\theta]_\infty$ = −40000 deg·cm^2·dmol^{-1} is the mean residue ellipticity at 222 nm of an infinitely long α-helix segment; n is the number of residues (n = 11 for XAO); k is a parameter that accounts for the end effects, since the end residues cannot effectively form α-helix conformations. k can varies from 4.6 to 6.3.[59] For the 21-residue polyAla peptide AP, k was reported to be 7.6.[60] The large variance of k results in a large uncertainty of $[\theta]_H$ estimated for short peptides.

The inset of Figure 1A shows the dependence of the XAO 222 nm ellipticity on the SDS concentration in 0.1 M $NaClO_4$ at 20 °C. The sigmoid shaped titration curve clearly indicates that SDS concentrations <1 mM have little impact on the XAO conformation. XAO is dominated by PPII-like conformations and shows a 222 nm mean residue ellipticity $[\theta]_P$ = −850 deg·cm^2·dmol^{-1}. The PPII to α-helix transition midpoint occurs at ∼3 mM SDS. Above 10 mM SDS, the α-helix conformation "saturates" with a 222 nm mean residue ellipticity of −12800 deg·cm^2·dmol^{-1}. We assign this value to a helical fraction of 0.69 that we calculated from the UVRR spectra (see below), and calculate $[\theta]_H$ = −18200 deg·cm^2·dmol^{-1}. This value is much more negative than that found for XAO in TFE,[57] indicating that, as expected, the maximum helical state is not achieved in TFE. The k parameter estimated from eq 4 is 6.0.

XAO $^1H_\alpha$ NMR Spectra. Figure 1B shows the one-dimensional $^1H_\alpha$ NMR spectra of XAO at different SDS concentrations in 0.1 M $NaClO_4$ aqueous solutions. The $^1H_\alpha$ NMR peaks of XAO overlap. In the absence of SDS, the $^1H_\alpha$ chemical shifts range from 4.18−4.42. The addition of 0.5 mM SDS does not affect the resonances of XAO (The triplet at ∼4.0 ppm arises from SDS). As the SDS concentration increases, the peaks shift further upfield with a significantly changed pattern.

The $^1H_\alpha$ XAO chemical shifts are sensitive to secondary structure.[61−63] For the "random coil" conformation, the reference chemical shift is 4.26 for the $^1H_\alpha$ of both Ala and Lys.[63] Presumably the chemical shifts are somewhat larger for Dab and Orn than Lys due to the fewer methylene groups between the amine group and C_α in Dab and Orn. The $^1H_\alpha$ chemical shift for the PPII conformation differs little from "random coil".[64] In α-helices, the $^1H_\alpha$ chemical shifts of Ala and Lys decrease to 4.03 and 3.99, respectively.[63] Our observed upfield shifts of XAO $^1H_\alpha$ resonances upon addition of SDS indicate a transition of PPII to an α-helix-like conformation, supporting the conclusions obtained from the CD spectra.

UVRR Spectra of XAO Dependence on SDS Concentration. The UVRR spectra of XAO with and without 0.1 M

dx.doi.org/10.1021/jp504133m | J. Phys. Chem. B 2014, 118, 10565−10575

$NaClO_4$ are essentially identical (Figure S1), indicating that 0.1 M $NaClO_4$ has negligible impact on the XAO conformation. We measured the 204 nm excited UVRR spectra of 1.0 mM XAO at different SDS concentrations with 0.1 M $NaClO_4$ at room temperature.

Figure 1C shows the 204 nm excited XAO UVRR spectra. Without SDS, the XAO UVRR spectrum shows an Am I band at ~1660 cm^{-1}, an Am II band at ~1550 cm^{-1}, overlapped with an interfering molecular oxygen band at 1556 cm^{-1}, two C_α−H bending bands at ~1392 cm^{-1} and ~1373 cm^{-1}, and an Am III_3 band at ~1255 cm^{-1}. As the SDS concentration increases, the Am III_3 band frequency slightly upshifts, while the intensities of the Am III_3 band and the C_α−H bending bands significantly decrease, indicating that XAO undergoes a transition from a PPII-like conformation to α-helix-like conformations that show hypochromism. These XAO spectra can be modeled as the sum of XAO spectra without SDS and XAO spectra with 100 mM SDS, confirming that this transition appears spectroscopically as a two-state system. The UVRR results are fully consistent with the CD and NMR results.

The C_α−H bending vibrations are resonance enhanced due to their coupling with N−H bending in the PPII-like conformation.[65] In α-helix-like conformations, the C_α−H bending decouples from the N−H bending and disappears.[66] Therefore, the C_α−H bending band intensities are mainly contributed by the PPII-like conformation. Consequently, the C_α−H bending bands can be used to calculate the PPII and α-helical fractions based on two-state modeling.[60]

α-Helical Fractions Calculated from UVRR, CD, and $^1H_\alpha$ NMR. The difference spectrum, shown in Figure 1C, between the UVRR spectra of XAO at 20 mM SDS and 0 mM SDS shows a band at 1382 cm^{-1}, that can be assigned to the methyl group umbrella bending of the Ala side chains.[67−69] We expect that the relative intensity of this methyl group umbrella bending band at 1382 cm^{-1} is independent of the XAO conformation.

We fit the XAO C_α-H bending region (from 1350 to 1420 cm^{-1}) of the UVRR spectra at different SDS concentrations with three Lorentzians. Two Lorentzian bands at 1371 and 1394 cm^{-1} model the C_α−H bending band spectra of the 11 residues. A Lorentzian band at 1382 cm^{-1} models the Ala methyl group umbrella bending. Assuming there are only two states, the α-helix-like conformation and the PPII conformation, the PPII fraction can be calculated from the 1371 and 1394 cm^{-1} Lorentzian band intensities at different SDS concentrations. The α-helical fractions of 1.0 mM XAO at different SDS concentrations calculated from UVRR spectra are shown in Figure 1D.

When the SDS concentration is above 10 mM, XAO shows a "saturated" helical fraction of ~0.69 calculated from the UVRR. The "saturated" α-helical fraction of ~0.69 indicates that, on average, around 7.6 of the 11 residues in XAO peptide are α-helical. The 7.6 residue long helical segment most likely occurs as a single segment in the middle of the peptide. We use the "saturated" helical fraction of ~0.69 to estimate $[\theta]_H$ via eq 3. With this $[\theta]_H$ value, we can calculate the XAO helical fraction at any SDS concentration from the CD spectra. The calculated XAO helical fractions are shown in Figure 1D as well.

The chemical shifts of the XAO $^1H_\alpha$, as discussed above, depend upon the XAO conformation. We calculate the first moment, which is the intensity weighed average chemical shift of the XAO $^1H_\alpha$ NMR bands at various SDS concentrations. The first moment decreases from 4.26 ppm in the absence of SDS to 4.12 ppm in 20 mM SDS. As shown by the CD and UVRR spectra, the XAO α-helix-PPII transition appears spectroscopically to be two-state. If the first moment of the PPII conformation is at 4.26 ppm, and the first moment of the SDS "saturated" XAO conformation (69% α-helix-like and 31% PPII) is at 4.12 ppm, assuming these two conformations are in the fast exchange limit, we can calculate the α-helical fractions of XAO in SDS aqueous solutions from the first moments of the XAO $^1H_\alpha$ NMR bands using

$$f_H = \frac{\delta - \delta_P}{\delta_H - \delta_P} \quad (5)$$

where δ is the first moment of the XAO $^1H_\alpha$ NMR band at a given SDS concentration. δ_P = 4.26 ppm is the XAO PPII conformation $^1H_\alpha$ NMR chemical shift and $\delta_H = ((4.12-4.26 \times 0.31)/0.69)$ ppm = 4.06 ppm is the XAO α-helix-like conformation $^1H_\alpha$ NMR chemical shift.

The calculated α-helical fractions from the first moments of the XAO $^1H_\alpha$ NMR spectra (eq 5) are shown in Figure 1D. These α-helical fractions are similar to those calculated from the CD and UVRR spectra.

The Effects of Long Alkyl Chains and Negatively Charged Surfactant Head Groups. Figure 2A shows the dependence of the 222 nm mean residue ellipticities of XAO on the concentrations of surfactants that have the same anionic sulfate headgroup as SDS but different alkyl chain lengths. SES

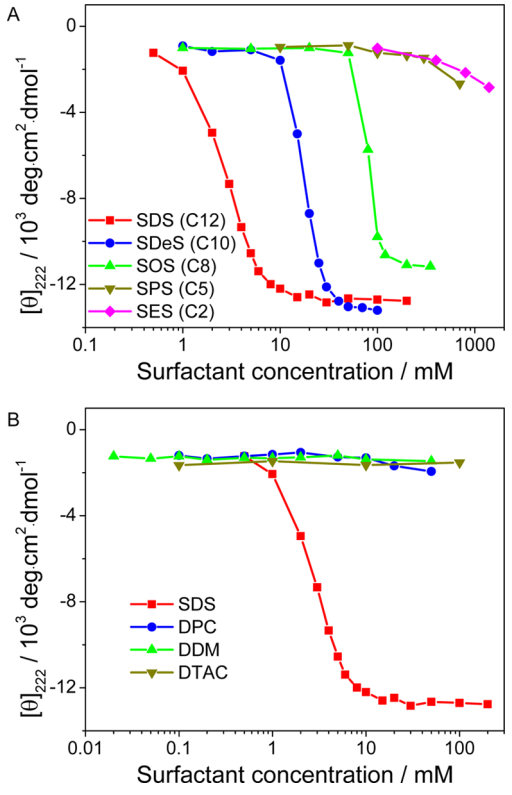

Figure 2. 222 nm ellipticities of 1.0 mM XAO in the presence of different surfactants. (A) Surfactants with different alkyl chain lengths. SDS: sodium dodecyl sulfate; SDeS: sodium decylsulfate; SOS: sodium octylsulfate; SPS: sodium pentylsulfate; SES: sodium ethylsulfate. (B) Surfactants with different head groups. SDS: sodium dodecyl sulfate; DPC: dodecylphosphocholine; DDM: dodecyl-β-D-maltoside; DTAC: dodecyltrimethylammonium chloride. Scheme 1 shows the molecular structures of these surfactants.

dx.doi.org/10.1021/jp504133m | J. Phys. Chem. B 2014, 118, 10565−10575

and SPS that possess relatively short alkyl chains have negligible impact on the XAO conformation even up to 0.7−1.0 M concentrations. Figure 2A shows that the surfactant concentration required to induce the XAO PPII to α-helix transition decreases as the surfactant alkyl chain length increases. The critical micelle concentrations (cmc's) of these surfactants are similarly dependent on chain length. The PPII to α-helix transition of XAO induced by SOS occurs between ∼50 mM to ∼120 mM with a midpoint at ∼80 mM, while the transition induced by SDeS occurs between ∼10 mM to ∼40 mM with a midpoint at ∼17 mM. The transition induced by SDS occurs between ∼1 mM to ∼10 mM with a midpoint at ∼3 mM.

Figure 2B compares the dependence of the XAO 222 nm mean residue ellipticities on the concentrations of surfactants with identical alkyl chain lengths but different head groups. These surfactants include anionic SDS, zwitterionic DPC, nonionic DDM and cationic DTAC (Scheme 1). Only SDS induces XAO to form α-helices, while the other three surfactants have little impact on the XAO conformation, even at concentrations much higher than their cmc's. This suggests that the anionic SDS interacts with cationic XAO to form α-helix conformations through electrostatic interactions with the four positively charged XAO side chains.

Scheme 1. Molecular Structures of Different Charged Head Group Surfactants

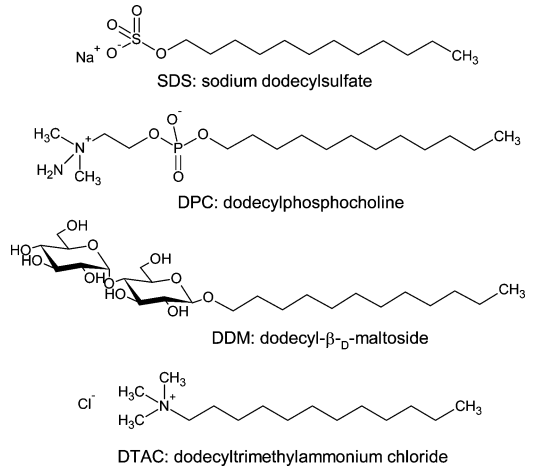

Diffusion Coefficients Measured by ^{1}H NMR DOSY Experiment. We used NMR DOSY to study the size and stoichiometry of the XAO−SDS aggregates by measuring the dependencies of the XAO and SDS diffusion coefficients on the SDS concentration.[70] The NMR DOSY spectra of 1.0 mM XAO at 0, 0.5 mM, 4.0 mM and 10 mM SDS concentrations are shown in Figure 3. The intensity of the resonance in the absence of a magnetic field gradient (I_0, that was calculated via eq 1) was plotted as a function of chemical shift at the top of contour plots. Along the right is a pseudo chromatograph, indicating the calculated diffusion coefficient associated with each chemical shift. The contour at δ = ∼4.7 ppm with D = ∼ 2 × 10^{-5}cm^2·s^{-1} derives from HOD in D_2O.

In the absence of SDS, Figure 3A shows XAO proton resonances at D = 2.0 × 10^{-6} cm^2·s^{-1}. Upon addition of SDS, the NMR spectrum shows SDS proton resonances. At 0.5 mM SDS, monomer SDS peak appears in the diffusion chromatograph at D = 4.3 × 10^{-6} cm^2·s^{-1} (Figure 3B). As the SDS concentration increases (Figure 3C,D), the diffusion coefficients of both the SDS and XAO species decrease, the XAO $^1H_\alpha$ resonances shift upfield, indicating α-helix formation as discussed above.

Figure 4A shows the dependence of the diffusion coefficients of 1.0 mM XAO and SDS in 0.1 M $NaClO_4$ on the SDS concentration. Also shown are the SDS diffusion coefficients in 0.1 M $NaClO_4$ (without XAO) as a function of SDS concentration. The SDS diffusion coefficient in the absence of XAO begins to decrease at ∼1.8 mM, indicating formation of micelles at a value similar to the cmc of SDS in 0.1 M NaCl (1.62 mM).[71]

Solutions containing 0.1 M $NaClO_4$, 1.0 mM XAO and <0.5 mM SDS, show constant XAO and SDS diffusion coefficients. The SDS diffusion coefficient is identical to that of 0.5 mM SDS in 0.1 M $NaClO_4$. These results indicate that XAO and SDS remain monomeric with D_{XAO} = (2.02 ± 0.01) × 10^{-6} cm^2·s^{-1} and D_{SDS} = (4.30 ± 0.03) × 10^{-6} cm^2·s^{-1}, respectively (Table 1).

Above 0.5 mM SDS, the XAO and SDS diffusion coefficients decrease, indicating the formation of XAO−SDS aggregates. This 0.5 mM SDS concentration is significantly lower than the cmc of SDS in 0.1 M $NaClO_4$ without XAO, indicating that XAO−SDS aggregates are formed between XAO monomers and SDS monomers. To confirm that the XAO−SDS aggregate formation does not require SDS micelles, we measured the dependence of the XAO CD spectra on SDS concentration in the absence of $NaClO_4$. Removal of $NaClO_4$ increases the SDS cmc to ∼8 mM.[71] If the XAO−SDS aggregation requires SDS micelle, it should show a different XAO conformational dependence on SDS concentration than in the presence of $NaClO_4$. In contrast, we observed a very similar SDS concentration dependence (Figure S2). This similar dependence confirms that XAO−SDS aggregation occurs between XAO monomers and SDS monomers.

At SDS concentration greater than ∼5 mM, the XAO diffusion coefficient remains constant at (6.9 ± 0.2) × 10^{-7} cm^2·s^{-1}. This constant XAO diffusion coefficient indicates that the XAO−SDS aggregates do not grow with increasing SDS concentration. The SDS diffusion coefficient decreases above ∼10 mM SDS due to the formation of SDS micelles (D_{Mic} = (6.0 ± 0.3) × 10^{-7} cm^2·s^{-1}).

Thus, aggregation between XAO and SDS monomers occurs at SDS concentrations between ∼0.5 mM to ∼5 mM SDS. Above 10 mM SDS, micelle formation occurs among SDS itself as evidenced by the decreased SDS diffusion coefficient. The diffusion coefficients of the XAO monomer, the SDS monomer, the XAO−SDS aggregate and the SDS micelle are listed in Table 1 along with the hydrodynamic radii estimated using the Stokes−Einstein equation that assumes spherical species.

Modeling of XAO and SDS Diffusion Coefficients. For a system in fast exchange, the apparent diffusion coefficient is a weighted average of the diffusion coefficients of all fast exchanging species

$$D^{App} = \frac{\sum_{i=1}^{n} q_i C_i D_i}{C^{Tot}} \quad (6)$$

where q_i, C_i, and D_i are the stoichiometry, the concentration, and the diffusion coefficient of the ith species; $C^{Tot} = \Sigma_{i=1}^{n} q_i C_i$ is the total concentration. From the diffusion coefficients of the XAO monomer, the SDS monomer, the XAO−SDS aggregate, and the SDS micelle listed in Table 1, we can use eq 6 to calculate the concentrations of XAO monomer (C_{XAO}) and

dx.doi.org/10.1021/jp504133m | J. Phys. Chem. B 2014, 118, 10565−10575

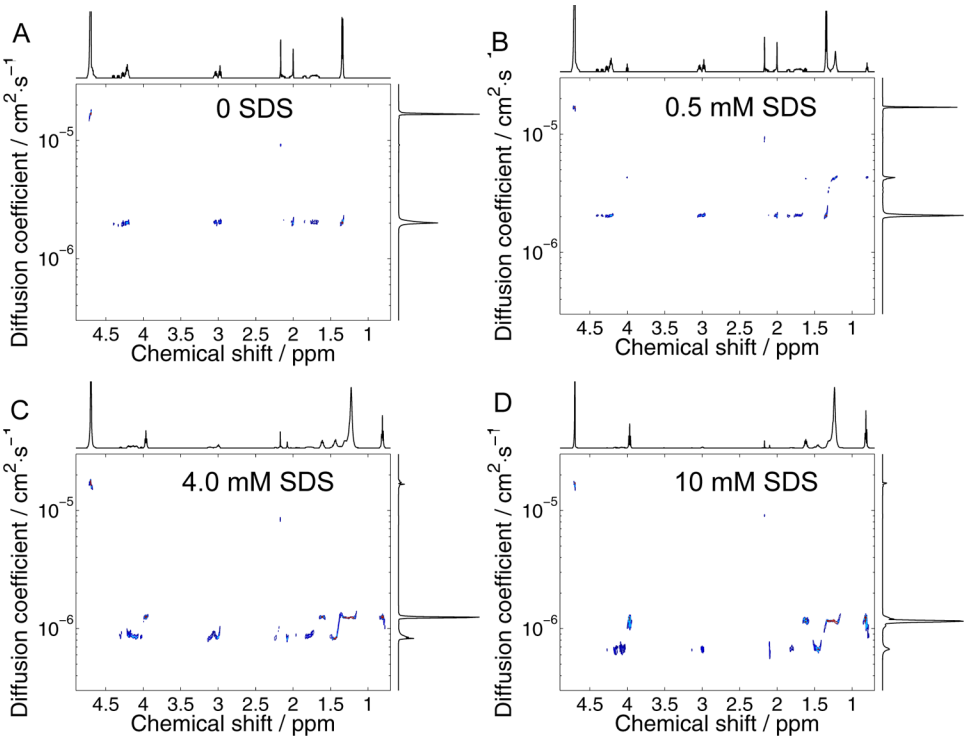

Figure 3. ^{1}H NMR DOSY spectra of XAO in (A) 0 mM, (B) 1.0 mM, (C) 4.0 mM and (D) 10 mM SDS solutions. All solutions contain 0.1 M $NaClO_4$. The calculated one-dimensional NMR spectrum without a magnetic field gradient is shown at the top of each figure. Along the right are pseudo chromatographs indicating the concentration of species as a function of diffusion coefficient.

SDS monomer (C_{SDS}), XAO−SDS aggregates (C_{Agg}), and SDS micelles (C_{Mic}) at each SDS concentration.

The binding equilibrium between XAO and SDS monomers, assuming only one aggregate species, can be described as

$$a\mathrm{XAO} + b\mathrm{SDS} \overset{K_{Agg}}{\rightleftharpoons} \mathrm{XAO}_a{-}\mathrm{SDS}_b$$

where K_{Agg} is the equilibrium constant for the XAO−SDS aggregate, and a and b are the numbers of XAO and SDS molecules in the XAO−SDS aggregate.

Fitting this model with species concentrations calculated using eq 6 at SDS < 5 mM finds $b/a = 3.9 \pm 0.3$, $a = 4.3 \pm 0.1$, and $K_{Agg} = (3.8 \pm 0.1) \times 10^4$ mM$^{-20.5}$. The ratio b/a suggests that in the aggregate, each XAO molecule is bound to four SDS monomers. The binding sites are most likely the four positively charged XAO side chains. Each XAO−SDS aggregate contains ∼4 XAO molecules and ∼16 SDS molecules.

As the SDS concentration increases, the XAO monomer becomes depleted. In contrast, the SDS monomer concentration increases until it reaches the cmc and micelles form. If m SDS monomers form a micelle

$$m\mathrm{SDS} \overset{K_{Mic}}{\rightleftharpoons} \mathrm{SDS}_m$$

where K_{Mic} is the micelle formation constant. Fitting this model with species concentrations calculated using eq 6 for SDS concentrations from 6 mM to 50 mM finds an aggregation number, $m = 38 \pm 8$ and $K_{Mic} = (1.1 \pm 5.5) \times 10^{-10}$ mM^{-37}.

Simple statistical mechanics predicts cmc = $K_{Mic}^{-(1/(m-1))}$.[72] Thus, we estimate cmc = 1.8 ± 0.1 mM, identical to the cmc of SDS measured in 0.1 M $NaClO_4$ solution (Figure 4A). This is close to the reported 1.62 mM cmc of SDS in 0.1 M NaCl.[71] The presence of 1.0 mM XAO does not appear to affect the SDS cmc equilibrium. However, XAO binds to SDS monomers and lowers the effective SDS monomer concentration, thus increasing the apparent total SDS concentration required to form SDS micelles.

Mechanism of SDS-Induced XAO α-Helix Formation. The diffusion coefficients (Figure 4A) and the solution species concentrations (Figure 4B) as a function of total SDS concentration were modeled using the parameters obtained above. The SDS concentration dependencies of solution species shown in Figure 4B can be divided into three regions: no interactions (<0.5 mM total SDS), XAO−SDS binding (0.5−5 mM total SDS), and SDS micellation (>5 mM total SDS).

Below 0.5 mM SDS, SDS does not bind to XAO or form micelles. The XAO monomer concentration remains constant as the SDS monomer concentration increases. Between 0.5 to 5 mM total SDS concentrations, SDS binds to XAO forming XAO−SDS aggregates prior to SDS micellation. The concentrations of aggregated XAO and aggregated SDS increase at the expense of XAO monomer. The SDS monomer concentration also increases. However, it remains below the cmc of SDS until ∼5 mM total SDS concentration. Above ∼5 mM total SDS, the micellation is triggered, and all species remain at constant concentrations, except the SDS micelle concentration increases.

Figure 5 compares the fraction of the aggregated XAO calculated from the diffusion coefficients, to the α-helical fractions calculated from the CD, $^1H_\alpha$-NMR and UVRR spectra. Upon scaling by 0.69, the fraction of the aggregated XAO exactly tracks the α-helical fraction, indicating that the XAO α-helix-like conformation correlates directly with XAO−SDS aggregation. However, in the XAO−SDS aggregates, some of the XAO residues, most likely the flanking Orn and Dab, remain in a PPII conformation.

dx.doi.org/10.1021/jp504133m | J. Phys. Chem. B 2014, 118, 10565−10575

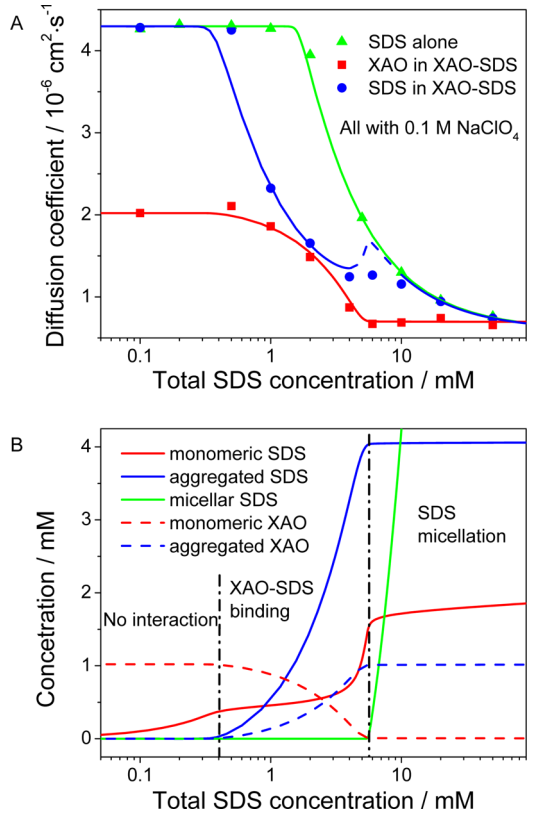

Figure 4. (A) Diffusion coefficients of 1.0 mM XAO and SDS in XAO−SDS solution and the diffusion coefficients of pure SDS in aqueous solution. All solutions contain 0.1 M $NaClO_4$. The data were experimentally measured by PFG-NMR; the curves are calculated by using parameters obtained from experimental data. (B) Calculated concentrations of different species in XAO−SDS solutions by using parameters obtained from experimental data.

Table 1. Diffusion Coefficients and Hydrodynamic Radius of Species in XAO−SDS Solution

species	diffusion coefficient[a]/10^{-6} $cm^2 \cdot s^{-1}$	hydrodynamic radius[b]/Å
XAO monomer	2.02 ± 0.01	9.8 ± 0.1
XAO−SDS aggregate	0.69 ± 0.02	29 ± 1
SDS monomer	4.30 ± 0.03	4.6 ± 0.1
SDS micelle	0.60 ± 0.03[c]	33 ± 2

[a]Measured at 25 °C in D_2O in the presence of 0.1 M $NaClO_4$ by PFG-NMR. [b]Calculated from diffusion coefficient using Stokes−Einstein equation $D = (k_BT/6\pi\eta r)$, where η = 1.098 mPa·s is the D_2O viscosity[80] at 25 °C. [c]Obtained by extrapolating the SDS diffusion coefficient to infinite SDS concentration in 0.1 M $NaClO_4$ without XAO.

Figure 6 shows a schematic model for the interactions between XAO and SDS that lead to α-helix formation. The negatively charged head groups of the SDS monomers electrostatically bind to the four XAO positively charged side chains. This significantly reduces electrostatic repulsion between Dab and Orn side chains and allows XAO to adopt the more compact α-helix-like conformations from the extended PPII conformation. The XAO−SDS_4 aggregates further associate with each other to form XAO_4−SDS_{16} aggregates. This results in a hydrophobic inner core comprised of the SDS alkyl groups, while one face of the α-helix backbone

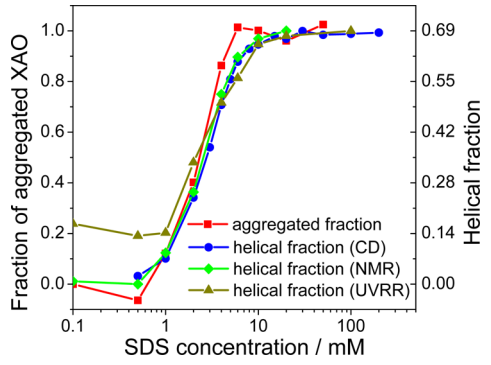

Figure 5. Comparison between fractions of aggregated XAO and α-helical XAO as determined by CD, NMR, and UVRR.

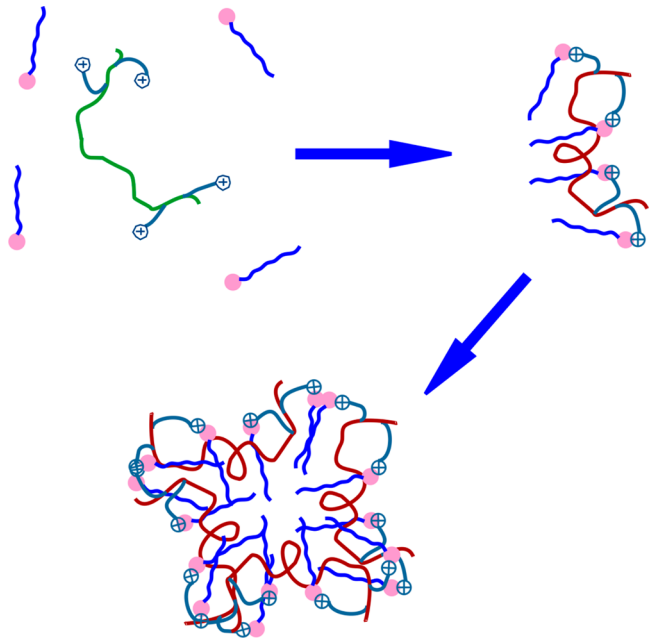

Figure 6. Mechanism of the XAO_4−SDS_{16} aggregation and the formation of XAO α-helix-like conformations. The four SDS alkyl chains bound to each XAO partition into a hydrophobic core that minimizes the hydrophobic area exposed to water. Neutralization of the flanking XAO charges enables α-helix formation such that one α-helix peptide face is buried within the hydrophobic core while the other face is in contact with the water environment.

is probably exposed to water medium. The other face of the XAO α-helix backbone is buried within the hydrophobic inner core. This stabilizes the α-helix formed by protecting the backbone hydrogen bonds.

Our results expose some of the fundamental interactions between some IDPs/AMPs and lipid systems. Our results show that charged side chains of IDPs/AMPs electrostatically bind to oppositely charged lipids, forming stable aggregates involving multiple peptides and lipids. This aggregation causes peptide partial dehydration, which increases α-helix stability as shown previously.[73] The formation of peptide-lipid aggregates also increases the effective local peptide concentration. This enables shorter range interpeptide interactions that can facilitate peptide aggregation.[5−7,74,75] Indeed, we observed large XAO aggregates in solutions containing 1 mM to 10 mM SDS concentration (1 < [SDS]/[XAO] < 10) after incubation at

dx.doi.org/10.1021/jp504133m | J. Phys. Chem. B 2014, 118, 10565−10575

room temperature for 3 days. In contrast, aggregation does not occur in pure XAO solution during this period.

Ramachandran ψ Angle Distributions of XAO in SDS Solution. The UVRR spectra contain information on the aggregated XAO conformations. By subtracting appropriate amounts of the measured PPII-like conformation UVRR spectrum, we can calculate the pure α-helix-like spectrum associated with the aggregated XAO at each SDS concentration. The pure α-helix-like spectra at different SDS concentrations are essentially identical (Figure S3), although there is somewhat less inhomogeneous broadening at higher SDS concentrations. We thus averaged over these calculated pure α-helix-like spectra at different SDS concentrations ($\mathbf{S}_\alpha(\upsilon,C_{SDS})$) weighted by their respective α-helical fractions ($f_\alpha(C_{SDS})$):

$$\mathbf{S}_\alpha(\upsilon) = \frac{\sum_{C_{SDS}} f_\alpha(C_{SDS})\mathbf{S}_\alpha(\upsilon, C_{SDS})}{\sum_{C_{SDS}} f_\alpha(C_{SDS})} \quad (7)$$

The averaged α-helix-like UVRR spectrum ($\mathbf{S}_\alpha(\upsilon)$) of aggregated XAO is shown in Figure 7. The Am III_3 band of

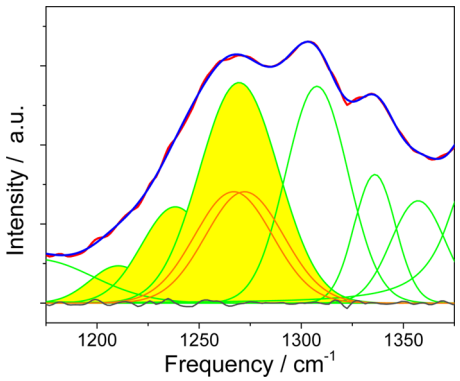

Figure 7. Bands resolved Am III region of the room temperature pure α-helix-like UVRR spectrum of XAO−SDS aggregates. This pure α-helix-like XAO−SDS aggregate UVRR spectrum is calculated by averaging the essentially identical pure α-helix-like XAO UVRR spectra at different SDS concentrations as weighted by their respective α-helical fractions. The α-helix-like UVRR spectrum at each SDS concentration is calculated by subtracting the PPII spectrum contribution. The Am III_3 deconvoluted bands are shown in yellow. The two presumed identical ~1270 cm^{-1} Am III_3 Gaussian bands derive from the C-terminal and N-terminal peptide bonds in the α-helix segment.

this pure α-helix-like UVRR spectrum can be modeled by three Gaussian bands at ~1210 cm^{-1}, ~1238 cm^{-1} and ~1270 cm^{-1}. The ~1210 and ~1238 cm^{-1} bands probably resulted from turn structures, while the ~1270 cm^{-1} band likely originates from α-helix-like conformations.

At 20 °C, the Am III_3 band frequency depends on both the ψ Ramachandran dihedral angle and peptide bond hydrogen bonding.[65,76]

$$\upsilon = \upsilon_0 - 54\ cm^{-1} \sin(\psi + 26°) \quad (8)$$

where υ_0 depends on the peptide bond hydrogen bonding. To calculate the ψ angle, υ_0 must be determined from the state of the peptide bond hydrogen bonding. Mikhonin et al. specified υ_0 for a number of peptide bond hydrogen bonding states.[77] Table 2 lists the relevant peptide bond hydrogen bonding states in an α-helix segment and their respective υ_0 values.

Table 2. Hydrogen Bonding States of Peptide Bonds in Aqueous Solution

peptide bond type	number of peptide bonds	hydrogen bond donor	hydrogen bond acceptor	υ_0/cm^{-1} (at 20 °C)[a]
N-terminus in an α-helix	4	H_2O	CO	1251.4
center in an α-helix	$n-8$	NH	CO	1244
C-terminus in an α-helix	4	NH	H_2O	1246
in PPII-like conformation	-	NH	H_2O	1253.8
		H_2O	CO	
turns	-	unknown	unknown	1248.8

[a]Values are estimated from ref 77

For aggregated XAO, we calculated above from the CD and UVRR that 7.6 residues occur in α-helix-like conformations. Thus, there are essentially no peptide bonds where both the carbonyl and amino groups form intrapeptide hydrogen bonds. In the XAO α-helix-like conformations, there are approximately 4 N-terminal and 4 C-terminal peptide bonds. At room temperature (~20 °C), the υ_0 difference between N-terminal and C-terminal peptide bonds is 5.4 cm^{-1} (Table 2) due to their different hydrogen bonding states.[77] Therefore, we fit the ~1270 cm^{-1} AmIII_3 band to two Gaussian bands that are separated by 5.4 cm^{-1} with identical band areas and identical widths. The low frequency band (~1267 cm^{-1}) simulates the C-terminal peptide bonds, while the high frequency (~1272 cm^{-1}) band simulates the N-terminal peptide bonds (Figure 7).

We previously developed a method[77−79] to calculate the peptide ψ angle distribution from the measured Am III_3 band. The Am III_3 band of the UVRR spectra from single crystal peptides show a homogeneous bandwidth of 15 cm^{-1}.[78] We deconvolute the Am III_3 band into a set of Lorentzian bands that have a fwhm of 15 cm^{-1}. The corresponding ψ angle associated with the center frequency (υ_L) of each of these Lorentzian bands was calculated from eq 8.

The probability of an XAO peptide bond occurring at a particular ψ angle can be calculated from the intensity of the Lorentzian band at this ψ angle, $I(\psi)$:

$$P(\psi) = \frac{I(\psi)}{\Delta\psi \sum_\psi I(\psi)} \quad (9)$$

where $\Delta\psi$ is the resolution interval between ψ angles that are determined from the spacing ($\Delta\upsilon_L$) between deconvoluted Lorentzian frequencies υ_L. Rewriting eq 8:

$$\Delta\psi(\upsilon_L) = \frac{\Delta\upsilon_L}{\sqrt{(54 cm^{-1})^2 - (\upsilon_L - \upsilon_0)^2}} \quad (10)$$

In the absence of SDS, XAO peptide bonds exist in PPII-like conformations that are fully hydrogen bonded to water. Therefore, the deconvoluted Am III_3 band in this XAO UVRR spectrum can be used to calculate the ψ angle distributions of the PPII-like XAO−SDS aggregate conformations by using eq 8 with υ_0 = 1253.8 cm^{-1} at ~20 °C (Table 2).

The ψ angle distribution of the α-helix-like conformation can be calculated from the Am III_3 band of the XAO pure α-helix-like UVRR spectrum. To reflect the different hydrogen bonding states of peptide bonds, different υ_0 (Table 2) are used in eq 8 to calculate the ψ angles from Figure 7 deconvolved different Am III_3 bands.

dx.doi.org/10.1021/jp504133m | J. Phys. Chem. B 2014, 118, 10565−10575

The aggregated XAO ψ angle distributions shown in Figure 8 contain a PPII-like conformation centered at 153° and an α-helix-like region centered at ~ −43°. The α-helix-like region ψ angle distributions deviate from a single Gaussian distribution, indicating multiple α-helix-like conformational states.

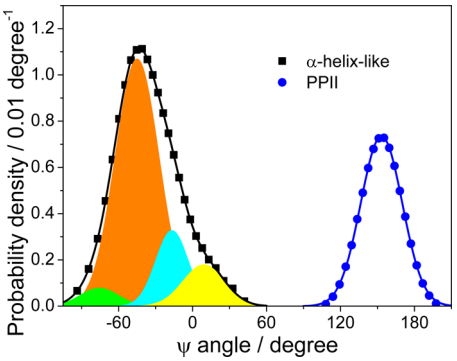

Figure 8. Ramachandran ψ angle distributions calculated for XAO−SDS aggregates from room temperature 204 nm excited UVRR spectra. The black envelope curve derives from the α-helix-like ψ angle distribution, that was fit to four Gaussians corresponding to π- (filled with green), α- (filled with orange) and 3_{10}- (filled with cyan) helices and turn structures (filled with yellow). The blue curve indicates PPII-like ψ angle distribution in the XAO−SDS aggregates.

Previously, Mikhonin resolved π-, α- and 3_{10}- helices of the AP peptide.[79] We thus fit the α-helix-like region ψ angle distributions of aggregated XAO to four normal distributions, modeling the ψ angle distributions as π-, α-, and 3_{10}- helices and a turn structure, respectively (Figure 8). Three conformational distributions are found at ψ = −76°, −45°, and −17°, in agreement with the expected α-helix-like ψ angles. An additional conformation is found at 9°, suggesting an additional turn conformation. Table 3 lists the conformations that we resolved in the aggregated XAO.

Table 3. Conformational States Resolved in the Aggregated XAO

conformation	center ψ angle/deg	standard deviation[a]/deg
π-helix	−76 ± 30	15 ± 8
α-helix	−45 ± 1	18 ± 5
3_{10}-helix	−17 ± 3	13 ± 3
turn structure	9 ± 6	17 ± 2
PPII	153 ± 1	17 ± 1

[a]Note torsional force constant is related to standard deviation of the distribution by $f = (RT/\sigma^2)$.

CONCLUSIONS

We used CD, NMR, and UVRR spectroscopy to demonstrate that XAO, which is predominately PPII conformation in aqueous solution, forms α-helix-like conformations in XAO−SDS aggregates. From the UVRR spectra, we calculated the ψ angle distributions of XAO−SDS aggregates. We resolved α-, π-, and 3_{10}- helix conformations, a turn structure and a PPII-like conformation. We studied the XAO−SDS aggregation by measuring the diffusion coefficients of the XAO monomer, the SDS monomer, and the XAO−SDS aggregate by using PFG-NMR spectroscopy. The XAO−SDS aggregates occur at SDS concentrations below the cmc. The SDS monomers bind to the XAO peptide, neutralizing the four positively charged side chains. Four XAO−SDS_4 further associate to from a stable aggregate of stoichiometry XAO_4−SDS_{16}, where the XAO adopts a predominantly α-helix-like conformation, which also contains turn and π- and 3_{10}- helices, rather than the predominant PPII conformation of the XAO monomers in aqueous solution. Our work suggests that the XAO−SDS aggregates form a hydrophobic core that minimizes the hydrophobic surface area in contact with water. Neutralization of the flanking charged side chains decreases the electrostatic penalty for α-helix formation. The exterior of the aggregate exposes the faces of the α-helix-like XAO peptide to water. This self-assembly mechanism may be relevant to the assembly of antimicrobial peptides and intrinsically disordered peptides into membranes.

ASSOCIATED CONTENT

Supporting Information

Supporting Information about the modeling of XAO−SDS interactions and SDS micellation is available free of charge via the Internet at http://pubs.acs.org.

AUTHOR INFORMATION

Corresponding Author

*Phone: (412)624-8570; e-mail: asher@pitt.edu.

Notes

The authors declare no competing financial interest.

ACKNOWLEDGMENTS

We are grateful to Dr. Lu Ma, Jonathan Wert and David Punihaole for helpful discussions. This work was supported in part by NIH grant 1RO1 EB009089.

REFERENCES

(1) Uversky, V. N. What Does It Mean to Be Natively Unfolded? *Eur. J. Biochem.* **2002**, *269* (1), 2−12.

(2) Caughey, B.; Lansbury, P. T. Protofibrils, Pores, Fibrils, and Neurodegeneration: Separating the Responsible Protein Aggregates from the Innocent Bystanders. *Annu. Rev. Neurosci.* **2003**, *26*, 267−298.

(3) Chiti, F.; Dobson, C. M. Protein Misfolding, Functional Amyloid, and Human Disease. *Annu. Rev. Biochem.* **2006**, *75*, 333−366.

(4) Uversky, V. N.; Oldfield, C. J.; Dunker, A. K. Intrinsically Disordered Proteins in Human Diseases: Introducing the D2 Concept. *Annu. Rev. Biophys.* **2008**, *37* (1), 215−246.

(5) Abedini, A.; Raleigh, D. P. A Critical Assessment of the Role of Helical Intermediates in Amyloid Formation by Natively Unfolded Proteins and Polypeptides. *Protein Eng. Des. Sel.* **2009**, *22* (8), 453−459.

(6) Abedini, A.; Raleigh, D. P. A Role for Helical Intermediates in Amyloid Formation by Natively Unfolded Polypeptides? *Phys. Biol.* **2009**, *6* (1), 015005.

(7) Butterfield, S. M.; Lashuel, H. A. Amyloidogenic Protein−Membrane Interactions: Mechanistic Insight from Model Systems. *Angew. Chem., Int. Ed.* **2010**, *49* (33), 5628−5654.

(8) Eliezer, D.; Kutluay, E.; Bussell, R., Jr; Browne, G. Conformational Properties of α-Synuclein in Its Free and Lipid-Associated States. *J. Mol. Biol.* **2001**, *307* (4), 1061−1073.

(9) Ahmad, M. F.; Ramakrishna, T.; Raman, B.; Rao, C. M. Fibrillogenic and Non-fibrillogenic Ensembles of SDS-Bound Human α-Synuclein. *J. Mol. Biol.* **2006**, *364* (5), 1061−1072.

(10) Giehm, L.; Oliveira, C. L. P.; Christiansen, G.; Pedersen, J. S.; Otzen, D. E. SDS-Induced Fibrillation of α-Synuclein: An Alternative Fibrillation Pathway. *J. Mol. Biol.* **2010**, *401* (1), 115−133.

(11) Dikiy, I.; Eliezer, D. Folding and Misfolding of α-Synuclein on Membranes. *Biochim. Biophys. Acta, Biomembr.* **2012**, *1818* (4), 1013−1018.
(12) Marcinowski, K. J.; Shao, H.; Clancy, E. L.; Zagorski, M. G. Solution Structure Model of Residues 1−28 of the Amyloid β-Peptide When Bound to Micelles. *J. Am. Chem. Soc.* **1998**, *120* (43), 11082−11091.
(13) Shao, H.; Jao, S.-c.; Ma, K.; Zagorski, M. G. Solution Structures of Micelle-Bound Amyloid β-(1−40) and β-(1−42) Peptides of Alzheimer's Disease. *J. Mol. Biol.* **1999**, *285* (2), 755−773.
(14) Terzi, E.; Hölzemann, G.; Seelig, J. Interaction of Alzheimer β-Amyloid Peptide(1−40) with Lipid Membranes. *Biochemistry* **1997**, *36* (48), 14845−14852.
(15) Okada, T.; Wakabayashi, M.; Ikeda, K.; Matsuzaki, K. Formation of Toxic Fibrils of Alzheimer's Amyloid β-Protein-(1−40) by Monosialoganglioside GM1, a Neuronal Membrane Component. *J. Mol. Biol.* **2007**, *371* (2), 481−489.
(16) Matsuzaki, K. Physicochemical Interactions of Amyloid β-Peptide with Lipid Bilayers. *Biochim. Biophys. Acta., Biomembr.* **2007**, *1768* (8), 1935−1942.
(17) Olofsson, A.; Borowik, T.; Gröbner, G.; Sauer-Eriksson, A. E. Negatively Charged Phospholipid Membranes Induce Amyloid Formation of Medin via an α-Helical Intermediate. *J. Mol. Biol.* **2007**, *374* (1), 186−194.
(18) Jayasinghe, S. A.; Langen, R. Lipid Membranes Modulate the Structure of Islet Amyloid Polypeptide. *Biochemistry* **2005**, *44* (36), 12113−12119.
(19) Knight, J. D.; Hebda, J. A.; Miranker, A. D. Conserved and Cooperative Assembly of Membrane-Bound α-Helical States of Islet Amyloid Polypeptide. *Biochemistry* **2006**, *45* (31), 9496−9508.
(20) Lashuel, H. A.; Hartley, D.; Petre, B. M.; Walz, T.; Lansbury, P. T. Neurodegenerative Disease: Amyloid Pores from Pathogenic Mutations. *Nature* **2002**, *418* (6895), 291−291.
(21) Last, N. B.; Miranker, A. D. Common Mechanism Unites Membrane Poration by Amyloid and Antimicrobial Peptides. *Proc. Natl. Acad. Sci. U. S. A.* **2013**, *110* (16), 6382−6387.
(22) Lashuel, H. A.; Lansbury, P. T. Are Amyloid Diseases Caused by Protein Aggregates That Mimic Bacterial Pore-Forming Toxins? *Q. Rev. Biophys.* **2006**, *39* (02), 167−201.
(23) Soscia, S. J.; Kirby, J. E.; Washicosky, K. J.; Tucker, S. M.; Ingelsson, M.; Hyman, B.; Burton, M. A.; Goldstein, L. E.; Duong, S.; Tanzi, R. E.; et al. The Alzheimer's Disease-Associated Amyloid β-Protein Is an Antimicrobial Peptide. *PLoS One* **2010**, *5* (3), e9505.
(24) Oren, Z.; Shai, Y. Mode of Action of Linear Amphipathic α-Helical Antimicrobial Peptides. *Pept. Sci.* **1998**, *47* (6), 451−463.
(25) Dathe, M.; Wieprecht, T. Structural Features of Helical Antimicrobial Peptides: Their Potential to Modulate Activity on Model Membranes and Biological Cells. *Biochim. Biophys. Acta., Biomembr.* **1999**, *1462* (1−2), 71−87.
(26) Tossi, A.; Sandri, L.; Giangaspero, A. Amphipathic, α-Helical Antimicrobial Peptides. *Pept. Sci.* **2000**, *55* (1), 4−30.
(27) Powers, J.-P. S.; Hancock, R. E. W. The Relationship between Peptide Structure and Antibacterial Activity. *Peptides* **2003**, *24* (11), 1681−1691.
(28) Zelezetsky, I.; Tossi, A. α-Helical Antimicrobial Peptides—Using a Sequence Template to Guide Structure−Activity Relationship Studies. *Biochim. Biophys. Acta., Biomembr.* **2006**, *1758* (9), 1436−1449.
(29) Johansson, J.; Gudmundsson, G. H.; Rottenberg, M. n. E.; Berndt, K. D.; Agerberth, B. Conformation-Dependent Antibacterial Activity of the Naturally Occurring Human Peptide LL-37. *J. Biol. Chem.* **1998**, *273* (6), 3718−3724.
(30) Park, C. B.; Yi, K.-S.; Matsuzaki, K.; Kim, M. S.; Kim, S. C. Structure−Activity Analysis of Buforin II, a Histone H2A-Derived Antimicrobial Peptide: The Proline Hinge is Responsible for the Cell-Penetrating Ability of Buforin II. *Proc. Natl. Acad. Sci. U. S. A.* **2000**, *97* (15), 8245−8250.
(31) Park, Y.; Park, S.-C.; Park, H.-K.; Shin, S. Y.; Kim, Y.; Hahm, K.-S. Structure-Activity Relationship of HP (2−20) Analog Peptide: Enhanced Antimicrobial Activity by N-terminal Random Coil Region Deletion. *Pept. Sci.* **2007**, *88* (2), 199−207.
(32) Uversky, V. N.; Gillespie, J. R.; Fink, A. L. Why Are "Natively Unfolded" Proteins Unstructured under Physiologic Conditions? *Proteins: Struct., Funct., Bioinf.* **2000**, *41* (3), 415−427.
(33) Oldfield, C. J.; Cheng, Y.; Cortese, M. S.; Brown, C. J.; Uversky, V. N.; Dunker, A. K. Comparing and Combining Predictors of Mostly Disordered Proteins. *Biochemistry* **2005**, *44* (6), 1989−2000.
(34) Shi, Z. S.; Chen, K.; Liu, Z. G.; Kallenbach, N. R. Conformation of the Backbone in Unfolded Proteins. *Chem. Rev.* **2006**, *106* (5), 1877−1897.
(35) Shi, Z. S.; Olson, C. A.; Rose, G. D.; Baldwin, R. L.; Kallenbach, N. R. Polyproline II Structure in a Sequence of Seven Alanine Residues. *Proc. Natl. Acad. Sci. U. S. A.* **2002**, *99* (14), 9190−9195.
(36) Tompa, P. Intrinsically Unstructured Proteins. *Trends Biochem. Sci.* **2002**, *27* (10), 527−533.
(37) Kjaergaard, M.; Nørholm, A. B.; Hendus-Altenburger, R.; Pedersen, S. F.; Poulsen, F. M.; Kragelund, B. B. Temperature-Dependent Structural Changes in Intrinsically Disordered Proteins: Formation of α-Helices or Loss of Polyproline II? *Protein Sci.* **2010**, *19* (8), 1555−1564.
(38) Adzhubei, A. A.; Sternberg, M. J. E.; Makarov, A. A. Polyproline-II Helix in Proteins: Structure and Function. *J. Mol. Biol.* **2013**, *425* (12), 2100−2132.
(39) Otvos, J. L. The Short Proline-Rich Antibacterial Peptide Family. *Cell. Mol. Life Sci.* **2002**, *59* (7), 1138−1150.
(40) Ferreon, A. C. M.; Gambin, Y.; Lemke, E. A.; Deniz, A. A. Interplay of α-Synuclein Binding and Conformational Switching Probed by Single-Molecule Fluorescence. *Proc. Natl. Acad. Sci. U. S. A.* **2009**, *106* (14), 5645−5650.
(41) Jalili, S.; Akhavan, M. Study of the Alzheimer's Aβ40 Peptide in SDS Micelles Using Molecular Dynamics Simulations. *Biophys. Chem.* **2011**, *153* (2−3), 179−186.
(42) Nanga, R. P. R.; Brender, J. R.; Vivekanandan, S.; Ramamoorthy, A. Structure and Membrane Orientation of IAPP in Its Natively Amidated Form at Physiological pH in a Membrane Environment. *Biochim. Biophys. Acta., Biomembr.* **2011**, *1808* (10), 2337−2342.
(43) Schibli, D. J.; Hwang, P. M.; Vogel, H. J. Structure of the Antimicrobial Peptide Tritrpticin Bound to Micelles: A Distinct Membrane-Bound Peptide Fold. *Biochemistry* **1999**, *38* (51), 16749−16755.
(44) Rozek, A.; Friedrich, C. L.; Hancock, R. E. W. Structure of the Bovine Antimicrobial Peptide Indolicidin Bound to Dodecylphosphocholine and Sodium Dodecyl Sulfate Micelles. *Biochemistry* **2000**, *39* (51), 15765−15774.
(45) Park, S.; Park, S.-H.; Ahn, H.-C.; Kim, S.; Kim, S. S.; Lee, B. J.; Lee, B.-J. Structural Study of Novel Antimicrobial Peptides, Nigrocins, Isolated from Rana Nigromaculata. *FEBS Lett.* **2001**, *507* (1), 95−100.
(46) Li, X.; Li, Y.; Han, H.; Miller, D. W.; Wang, G. Solution Structures of Human LL-37 Fragments and NMR-Based Identification of a Minimal Membrane-Targeting Antimicrobial and Anticancer Region. *J. Am. Chem. Soc.* **2006**, *128* (17), 5776−5785.
(47) Japelj, B.; Zorko, M.; Majerle, A.; Pristovšek, P.; Sanchez-Gomez, S.; de Tejada, G. M.; Moriyon, I.; Blondelle, S. E.; Brandenburg, K.; Andrä, J.; et al. The Acyl Group as the Central Element of the Structural Organization of Antimicrobial Lipopeptide. *J. Am. Chem. Soc.* **2007**, *129* (5), 1022−1023.
(48) Oladepo, S. A.; Xiong, K.; Hong, Z.; Asher, S. A. Elucidating Peptide and Protein Structure and Dynamics: UV Resonance Raman Spectroscopy. *J. Phys. Chem. Lett.* **2011**, *2* (4), 334−344.
(49) Oladepo, S. A.; Xiong, K.; Hong, Z.; Asher, S. A.; Handen, J.; Lednev, I. K. UV Resonance Raman Investigations of Peptide and Protein Structure and Dynamics. *Chem. Rev.* **2012**, *112* (5), 2604−2628.
(50) Bykov, S.; Lednev, I.; Ianoul, A.; Mikhonin, A.; Munro, C.; Asher, S. A. Steady-State and Transient Ultraviolet Resonance Raman Spectrometer for the 193−270 nm Spectral Region. *Appl. Spectrosc.* **2005**, *59* (12), 1541−1552.

(51) Cotts, R. M.; Hoch, M. J. R.; Sun, T.; Markert, J. T. Pulsed Field Gradient Stimulated Echo Methods for Improved NMR Diffusion Measurements in Heterogeneous Systems. *J. Magn. Reson.* **1989**, *83* (2), 252−266.
(52) Wu, D. H.; Chen, A. D.; Johnson, C. S. An Improved Diffusion-Ordered Spectroscopy Experiment Incorporating Bipolar-Gradient Pulses. *J. Magn. Reson. A* **1995**, *115* (2), 260−264.
(53) Stejskal, E. O.; Tanner, J. E. Spin Diffusion Measurements: Spin Echoes in the Presence of a Time-Dependent Field Gradient. *J. Chem. Phys.* **1965**, *42* (1), 288−292.
(54) Tanner, J. E. Use of the Stimulated Echo in NMR Diffusion Studies. *J. Chem. Phys.* **1970**, *52* (5), 2523−2526.
(55) Nilsson, M.; Morris, G. A. Speedy Component Resolution: An Improved Tool for Processing Diffusion-Ordered Spectroscopy Data. *Anal. Chem.* **2008**, *80* (10), 3777−3782.
(56) Makowska, J.; Rodziewicz-Motowidło, S.; Bagińska, K.; Vila, J. A.; Liwo, A.; Chmurzyński, L.; Scheraga, H. A. Polyproline II Conformation is One of Many Local Conformational States and Is Not an Overall Conformation of Unfolded Peptides and Proteins. *Proc. Natl. Acad. Sci. U. S. A.* **2006**, *103* (6), 1744−1749.
(57) Makowska, J.; Rodziewicz-MotowidBo, S.; Baginska, K.; Makowski, M.; Vila, J. A.; Liwo, A.; Chmurzynski, L.; Scheraga, H. A. Further Evidence for the Absence of Polyproline II Stretch in the XAO Peptide. *Biophys. J.* **2007**, *92* (8), 2904−2917.
(58) Chen, Y.-H.; Yang, J. T.; Chau, K. H. Determination of the Helix and b-Form of Proteins in Aqueous Solution by Circular Dichroism. *Biochemistry* **1974**, *13* (16), 3350.
(59) Gans, P. J.; Lyu, P. C.; Manning, M. C.; Woody, R. W.; Kallenbach, N. R. The Helix-Coil Transition in Heterogeneous Peptides with Specific Side Chain Interactions: Theory and Comparison with CD Spectral Data. *Biopolymers* **1991**, *31* (13), 1605−1614.
(60) Lednev, I. K.; Karnoup, A. S.; Sparrow, M. C.; Asher, S. A. α-Helix Peptide Folding and Unfolding Activation Barriers: A Nanosecond UV Resonance Raman Study. *J. Am. Chem. Soc.* **1999**, *121* (35), 8074−8086.
(61) Wishart, D. S.; Sykes, B. D.; Richards, F. M. Relationship between Nuclear Magnetic Resonance Chemical Shift and Protein Secondary Structure. *J. Mol. Biol.* **1991**, *222* (2), 311−333.
(62) Mielke, S. P.; Krishnan, V. V. Characterization of Protein Secondary Structure from NMR Chemical Shifts. *Prog. NMR. Spec.* **2009**, *54* (3−4), 141−165.
(63) Wishart, D. S. Interpreting Protein Chemical Shift Data. *Prog. NMR. Spec.* **2011**, *58* (1−2), 62−87.
(64) Lam, S. L.; Hsu, V. L. NMR Identification of Left-Handed Polyproline Type II Helices. *Biopolymers* **2003**, *69* (2), 270−281.
(65) Asher, S. A.; Ianoul, A.; Mix, G.; Boyden, M. N.; Karnoup, A.; Diem, M.; Schweitzer-Stenner, R. Dihedral Ψ Angle Dependence of the Amide III Vibration: A Uniquely Sensitive UV Resonance Raman Secondary Structural Probe. *J. Am. Chem. Soc.* **2001**, *123* (47), 11775−11781.
(66) Wang, Y.; Purrello, R.; Jordan, T.; Spiro, T. G. UVRR Spectroscopy of the Peptide Bond. 1. Amide S, a Nonhelical Structure Marker, Is a C_a−H Bending Mode. *J. Am. Chem. Soc.* **1991**, *113* (17), 6359−6368.
(67) Lee, S.-H.; Krimm, S. Ab Initio-Based Vibrational Analysis of α-Poly(L-alanine). *Biopolymers* **1998**, *46* (5), 283−317.
(68) Mikhonin, A. V.; Ahmed, Z.; Ianoul, A.; Asher, S. A. Assignments and Conformational Dependencies of the Amide III Peptide Backbone UV Resonance Raman Bands. *J. Phys. Chem. B* **2004**, *108* (49), 19020−19028.
(69) Mikhonin, A. V.; Asher, S. A. Uncoupled Peptide Bond Vibrations in α-Helical and Polyproline II Conformations of Polyalanine Peptides. *J. Phys. Chem. B* **2005**, *109* (7), 3047−3052.
(70) Orfi, L.; Lin, M.; Larive, C. K. Measurement of SDS Micelle−Peptide Association Using ^{1}H NMR Chemical Shift Analysis and Pulsed-Field Gradient NMR Spectroscopy. *Anal. Chem.* **1998**, *70* (7), 1339−1345.
(71) Rosen, M. J. *Surfactants and Interfacial Phenomena*, 3rd ed.; Wiley: Hoboken , NJ, 2004.
(72) Dill, K. A.; Bromberg, S. *Molecular Driving Forces*; Garland Science: New York, 2003; p 666.
(73) Mukherjee, S.; Chowdhury, P.; Gai, F. Infrared Study of the Effect of Hydration on the Amide I Band and Aggregation Properties of Helical Peptides. *J. Phys. Chem. B* **2007**, *111* (17), 4596−4602.
(74) Gorbenko, G. P.; Kinnunen, P. K. J. The Role of Lipid−Protein Interactions in Amyloid-Type Protein Fibril Formation. *Chem. Phys. Lipids* **2006**, *141* (1−2), 72−82.
(75) Byström, R.; Aisenbrey, C.; Borowik, T.; Bokvist, M.; Lindström, F.; Sani, M.-A.; Olofsson, A.; Gröbner, G. Disordered Proteins: Biological Membranes as Two-Dimensional Aggregation Matrices. *Cell Biochem. Biophys.* **2008**, *52* (3), 175−189.
(76) Myshakina, N. S.; Ahmed, Z.; Asher, S. A. Dependence of Amide Vibrations on Hydrogen Bonding. *J. Phys. Chem. B* **2008**, *112* (38), 11873−11877.
(77) Mikhonin, A. V.; Bykov, S. V.; Myshakina, N. S.; Asher, S. A. Peptide Secondary Structure Folding Reaction Coordinate: Correlation between UV Raman Amide III Frequency, Ψ Ramachandran Angle, and Hydrogen Bonding. *J. Phys. Chem. B* **2006**, *110* (4), 1928−1943.
(78) Asher, S. A.; Mikhonin, A. V.; Bykov, S. UV Raman Demonstrates That α-Helical Polyalanine Peptides Melt to Polyproline II Conformations. *J. Am. Chem. Soc.* **2004**, *126* (27), 8433−8440.
(79) Mikhonin, A. V.; Asher, S. A. Direct UV Raman Monitoring of 3_{10}-Helix and π-Bulge Premelting during α-Helix Unfolding. *J. Am. Chem. Soc.* **2006**, *128* (42), 13789−13795.
(80) Dean, J. A. *Lange's Handbook of Chemistry*, 15 ed.; McGraw-Hill, Inc: New York, 1999.